DYNAMIC STIFFNESS METHOD FOR INPLANE FREE VIBRATION OF ROTATING BEAMS INCLUDING CORIOLIS EFFECTS

J.R. Banerjee[a*] and D. Kennedy[b]

[a]School of Engineering and Mathematical Sciences, City University London

Northampton Square, London EC1V 0HB, UK

[b]Cardiff School of Engineering, Cardiff University

Queen's Buildings, The Parade, Cardiff CF24 3AA, UK

Abstract

The paper addresses the in-plane free vibration analysis of rotating beams using an exact dynamic stiffness method. The analysis includes the Coriolis effects in the free vibratory motion as well as the effects of an arbitrary hub radius and an outboard force. The investigation focuses on the formulation of the frequency dependent dynamic stiffness matrix to perform exact modal analysis of rotating beams or beam assemblies. The governing differential equations of motion, derived from Hamilton's principle, are solved using the Frobenius method. Natural boundary conditions resulting from the Hamiltonian formulation enable expressions for nodal forces to be obtained in terms of arbitrary constants. The dynamic stiffness matrix is developed by relating the amplitudes of the nodal forces to those of the corresponding responses, thereby eliminating the arbitrary constants. Then the natural frequencies and mode shapes follow from the application of the Wittrick-Williams algorithm. Numerical results for an individual rotating beam for cantilever boundary condition are given and some results are validated. The influences of Coriolis effects, rotational speed and hub radius on the natural frequencies and mode shapes are illustrated.

---

[*]Corresponding author. Email: j.r.banerjee@city.ac.uk, Tel. +44 (0) 2070408924, Fax +44 (0) 2070408566

1. Introduction

There are numerous engineering applications of rotating beams. Helicopter, compressor and turbine blades are some examples for which evaluation of natural frequencies and mode shapes is very important. In general, the cross-sections of these structures are very complex, but researchers have often made simplifying assumptions in order to carry out preliminary assessments and establish behavioural trends. Such simplified models often ignore the coupling between various modes of elastic deformations. For example, the free vibration behaviour of rotating beams has often been studied by considering only the bending deformation which generally dominates the behaviour of helicopter and wind turbine blades. Research based on this simplifying assumption that the beam deforms only in bending is, without doubt, restrictive. Nevertheless, there is some justification in doing such analysis which can give considerable insight into the problem and thus provides a useful basis for further research. The literature on the free vibration behaviour of rotating beams using only bending theory is surprisingly voluminous and has continued to grow to this day. The authors have compiled a selective sample of recent papers [1-16] which provide background information and useful cross-references on the subject.

Several of these publications rely on classical methods based on the solution of the governing differential equations and the subsequent imposition of boundary conditions, leading to the frequency equation [5, 11]. There are, however, some exceptions where finite element method (FEM) based solutions have also been reported [6, 13] along with the application of other methods such as the differential transform method [14, 15]. A significant contribution in recent years is the application of the dynamic stiffness method (DSM) [1, 4, 9] which extends the analysis to a much wider context, while at the same time ensuring exact results. The DSM is indeed a versatile tool because it has all the essential features of the FEM such as coordinate transformation, assembly procedure, sub-structuring, etc., but importantly, unlike the FEM, it permits exact eigenvalue analysis.

Although the DSM has been successfully applied to rotating beams [1, 4, 9], the important influence of the Coriolis effects arising from the in-plane rotational motion has not been included to date. However, it should be recognised that a handful of researchers [5, 11, 16] have included the Coriolis terms when investigating the free vibration behaviour of individual beams using the classical method, but without applying the DSM. These earlier studies have highlighted the effect of the Coriolis terms, particularly at high rotational speeds. Lin and

Hsiao [5] used d'Alembert's principle and the principle of virtual work to formulate the eigenproblem, whereas Lee and Sheu [11] used Hamilton's principle as a precursor to an exact power solution of the same problem. A notable contribution came from Huang *et al.* [16], who investigated the free vibration problem of a rotating Bernoulli-Euler beam inclined at an arbitrary angle to the axis of rotation. Their study included the influence of Coriolis effects, rotational angular velocity and slenderness ratio on the natural frequencies and mode shapes.

The current paper is partly motivated by these investigations, and fills an irritating gap in the DSM literature by providing free vibration solutions for rotating beams, including the Coriolis terms which essentially couple the axial and in-plane flexural deformations during the free vibratory motion. The dynamic stiffness matrix of a rotating beam exhibiting coupling between in-plane (lagwise) bending and axial deformations that occurs due to Coriolis terms is developed to investigate the free vibration characteristics. The investigation is carried out in the following steps.

(i) Hamilton's principle is applied to derive the governing differential equations of motion for in-plane free vibration of a rotating uniform beam with the inclusion of the Coriolis effects.

(ii) As a consequence of the Hamiltonian formulation the natural boundary conditions are recovered to obtain expressions for forces and moments.

(iii) The differential equations are solved by the Frobenius method of series solution.

(iv) Expressions for nodal responses (i.e. displacements and rotations) and loads (i.e. forces and moments) are obtained in explicit analytical form.

(v) Boundary conditions are imposed in algebraic form and the constants of the solution are eliminated to relate the amplitudes of nodal loads and responses, leading to the development of the frequency dependent dynamic stiffness matrix of the rotating beam.

(vi) The well-established algorithm of Wittrick and Williams [17] is applied to the dynamic stiffness matrix to solve the (transcendental) eigenvalue problem, yielding the natural frequencies and enabling the subsequent recovery of mode shapes.

(vii) A detailed parametric study is undertaken to compute numerical results by varying significant parameters, with particular emphasis on the rotational speed in order to capture the influence of the Coriolis effects.

(viii) Results for natural frequencies and mode shapes of some illustrative examples are discussed and wherever possible compared with published ones, and significant conclusions are drawn.

2. Dynamic Stiffness Formulation

Figure 1 shows the axis system of a typical rotating Bernoulli-Euler beam element of length L with its left-hand end at a distance r_i from the axis of rotation. Note that r_i may or may not be equal to the hub radius r_h, and also L may differ from the total length L_T of the beam, as shown in the figure. The beam is assumed to be rotating at a constant angular velocity Ω and has a doubly symmetric cross-section such as a rectangle or a circle etc. so that the bending and torsional motions as well as the in-plane and out-of-plane motions are uncoupled. In the right-handed Cartesian coordinate system, the origin is taken to be at the left-hand end of the beam element as shown, with the X-axis coinciding with the neutral axis of the beam in the undeflected position. The Z-axis is taken to be parallel to (but not necessarily coincident with) the axis of rotation while the Y-axis lies in the plane of rotation. Thus the principal axes of the beam cross-section are parallel to the Y and Z directions. The free vibratory motion of the beam is considered to occur in the X-Y plane (i.e. lag-wise motion). The flexure in the Y-direction is coupled with the axial motion in the X-direction through Coriolis effects. A schematic plan view of this element is shown in Figure 2 in which the X, Y and Z axes are fixed within the element, with the origin at its left-hand end. (Note that the out-of-plane free vibration of a rotating beam with no coupling between the flexural (or bending) motion with the axial (or extensional) motion has been dealt with by the first author by using the DSM in an earlier publication [1].) The axial and flexural rigidities of the beam are assumed to be EA and EI respectively, whereas the density of beam material is ρ and its cross-sectional area is A. In order to allow for the centrifugal forces developed in adjacent beam elements, the theory is generalised by including an outboard axial force T_0 at the outer end of the element,

as shown in Figure 2. For the element at the extreme outer end of the whole beam, see Figure 1, this force is clearly zero.

Referring to Figure 2, the time-independent centrifugal tension $T(x)$ at a distance x from the origin is given by [1, 4]

$$T(x) = \rho A \int_x^L \Omega^2 (r_h + x)\, dx + T_0 = \rho A \Omega^2 \left[r_h (L - x) + \frac{1}{2}(L^2 - x^2) \right] + T_0 \tag{1}$$

The governing differential equations of motion of the rotating beam can be derived using Hamilton's principle for which the expressions for kinetic ($\mathcal{T}$) and potential ($\mathcal{V}$) energies are fundamental prerequisites. Referring to Figure 2, it can be shown that $\mathcal{T}$ and $\mathcal{V}$ are given by [1, 5]

$$\mathcal{T} = \frac{\rho A}{2} \int_0^L \{(\dot{u} - \Omega v)^2 + (\dot{v} + \Omega u)^2\}\, dx \tag{2}$$

and

$$\mathcal{V} = \frac{EA}{2} \int_0^L (u')^2\, dx + \frac{EI}{2} \int_0^L (v'')^2\, dx + \frac{1}{2} \int_0^L T (v')^2\, dx \tag{3}$$

where u and v are (elastic) displacements of a point at a distance x from the origin in the X and Y directions respectively, an over dot represents differentiation with respect to time t and a prime denotes differentiation with respect to x.

Hamilton's principle states

$$\delta \int_{t_1}^{t_2} (\mathcal{T} - \mathcal{V})\, dt = 0 \tag{4}$$

where t_1 and t_2 are the time intervals in the dynamic trajectory, and δ is the usual variational operator.

Substituting the expressions for $\mathcal{T}$ and $\mathcal{V}$ from equations (2) and (3) into equation (4), using the variational operator and then carrying out integration by parts in the usual way yields the following governing differential equations of motion of the rotating beam.

$$EAu'' - \rho A\ddot{u} + 2\rho A\Omega\dot{v} + \rho A\Omega^2 u = 0 \tag{5}$$

$$EIv'''' + \rho A\ddot{v} + 2\rho A\Omega\dot{u} - \rho A\Omega^2 v - (Tv')' = 0 \tag{6}$$

The natural boundary conditions generated by the Hamiltonian formulation give the following time-dependent expressions for axial force (f) with tensile force positive, bending moment (m), with hogging moment positive and shear force (s), with clockwise shear positive [18].

$$f = EAu' ; \qquad m = -EIv'' ; \qquad s = EIv''' - Tv' \tag{7}$$

Assuming harmonic oscillation of the form

$$u = Ue^{i\omega t} \quad ; \qquad v = Ve^{i\omega t} \tag{8}$$

and writing

$$k_u = \frac{EA}{\rho A} \ ; \qquad k_v = \frac{EI}{\rho A} \tag{9}$$

equations (5) and (6) can be written with the help of equation (1) as

$$k_u U'' + (\omega^2 + \Omega^2)U + 2i\omega\Omega V = 0 \tag{10}$$

$$k_v V'''' - (\omega^2 + \Omega^2)V + 2i\omega\Omega U + \left\{\Omega^2\left[r_h(x-L) + \frac{1}{2}(x^2 - L^2)\right] + \frac{T_0}{\rho A}\right\}V'' + \Omega^2(r_h + x)V' = 0 \tag{11}$$

Substituting for V from equation (10) into equation (11) gives

$$k_u k_v U'''''' + \left\{k_v(\omega^2 + \Omega^2) + k_u\Omega^2\left[r_h(x-L) + \frac{1}{2}(x^2 - L^2)\right] + k_u\frac{T_0}{\rho A}\right\}U'''' + k_u\Omega^2(r_h + x)U''' + (\omega^2 + \Omega^2)\left\{\Omega^2\left[r_h(x-L) + \frac{1}{2}(x^2 - L^2)\right] - k_u + \frac{T_0}{\rho A}\right\}U'' + \Omega^2(\omega^2 + \Omega^2)(r_h + x)U' + [4\omega^2\Omega^2 - (\omega^2 + \Omega^2)^2]U = 0 \tag{12}$$

Making a change of variable from x to ξ where

$$\xi = x/L \tag{13}$$

equation (12) becomes

$$[D^6 + (c_1 + c_2\xi + c_3\xi^2)D^4 + (c_4 + c_5\xi)D^3 + (c_6 + c_7\xi + c_8\xi^2)D^2 + (c_9 + c_{10}\xi)D + c_{11}]U = 0 \tag{14}$$

where $D = d/d\xi$,

$$\left.\begin{aligned} &c_1 = \alpha_1 - \left[\alpha_3\left(r_0 + \frac{1}{2}\right) + \alpha_5\right]; \qquad c_2 = c_4 = \alpha_3 r_0; \qquad 2c_3 = c_5 = \alpha_3; \\ &c_6 = -\alpha_1\left[\alpha_3\left(r_0 + \frac{1}{2}\right) + \alpha_5\right] - \alpha_2; \quad c_7 = c_9 = \alpha_1\alpha_3 r_0; \quad 2c_8 = c_{10} = \alpha_1\alpha_3; \\ &c_{11} = -(\alpha_1\alpha_2 - 4\alpha_3\alpha_4); \\ &\alpha_1 = \frac{(\omega^2 + \Omega^2)L^2}{k_u}; \qquad \alpha_2 = \frac{(\omega^2 + \Omega^2)L^4}{k_v}; \qquad \alpha_3 = \frac{\Omega^2 L^4}{k_v}; \\ &\alpha_4 = \frac{\omega^2 L^2}{k_u}; \qquad \alpha_5 = \frac{T_0 L^2}{EI}; \qquad r_0 = \frac{r_h}{L} \end{aligned}\right\} \tag{15}$$

Similarly, substituting for U from equation (10) into equation (11) leads to

$$[D^6 + (c_1 + c_2\xi + c_3\xi^2)D^4 + (\bar{c}_4 + \bar{c}_5\xi)D^3 + (\bar{c}_6 + c_7\xi + c_8\xi^2)D^2 + (c_9 + c_{10}\xi)D + c_{11}]V = 0 \tag{16}$$

where

$$\bar{c}_4 = 3c_4; \qquad \bar{c}_5 = 3c_5; \qquad \bar{c}_6 = 3\alpha_3 + c_6 \tag{17}$$

Equations (14) and (16) are solved using the Frobenius method of series solution. Thus, by assuming

$$U(\xi) = \sum_{n=0}^{\infty} a_{n+1}\,\xi^{c+n} \tag{18}$$

$$V(\xi) = \sum_{n=0}^{\infty} b_{n+1}\,\xi^{\bar{c}+n} \tag{19}$$

where $a_1 \neq 0$, $b_1 \neq 0$, the starting indices c and $\bar{c}$ are determined from the indicial equations as follows.

Substituting equation (18) into equation (14) gives

$$\sum_{n=0}^{\infty} a_{n+1} \begin{Bmatrix} (c+n)(c+n-1)(c+n-2)(c+n-3)(c+n-4)(c+n-5)\xi^{c+n-6} \\ +(c+n)(c+n-1)(c+n-2)(c+n-3)c_1\xi^{c+n-4} \\ +(c+n)(c+n-1)(c+n-2)[c_2(c+n-3)+c_4]\xi^{c+n-3} \\ +(c+n)(c+n-1)[c_3(c+n-2)(c+n-3)+c_5(c+n-2)+c_6]\xi^{c+n-2} \\ +(c+n)[c_7(c+n-1)+c_9]\xi^{c+n-1} \\ +[c_8(c+n)(c+n-1)+c_{10}(c+n)+c_{11}]\xi^{c+n}=0 \end{Bmatrix} \tag{20}$$

Multiplying both sides by ξ^{-c+6} and expanding in powers of ξ gives

$$\begin{aligned} &a_1c(c-1)(c-2)(c-3)(c-4)(c-5) \\ &+a_2(c+1)c(c-1)(c-2)(c-3)(c-4)\xi \\ &+\begin{Bmatrix} a_3(c+2)(c+1)c(c-1)(c-2)(c-3) \\ +a_1c(c-1)(c-2)(c-3)c_1 \end{Bmatrix}\xi^2 \\ &+\begin{Bmatrix} a_4(c+3)(c+2)(c+1)c(c-1)(c-2) \\ +a_2(c+1)c(c-1)(c-2)c_1 \\ +a_1c(c-1)(c-2)[c_2(c-3)+c_4] \end{Bmatrix}\xi^3 \\ &+\begin{Bmatrix} a_5(c+4)(c+3)(c+2)(c+1)c(c-1) \\ +a_3(c+2)(c+1)c(c-1)c_1 \\ +a_2(c+1)c(c-1)[c_2(c-2)+c_4] \\ +a_1c(c-1)[c_3(c-2)(c-3)+c_5(c-2)+c_6] \end{Bmatrix}\xi^4 \\ &+\begin{Bmatrix} a_6(c+5)(c+4)(c+3)(c+2)(c+1)c \\ +a_4(c+3)(c+2)(c+1)cc_1 \\ +a_3(c+2)(c+1)c[c_2(c-2)+c_4] \\ +a_2(c+1)c[c_3(c-2)(c-3)+c_5(c-2)+c_6] \\ +a_1c[c_7(c-1)+c_9] \end{Bmatrix}\xi^5 \\ &+\sum_{n=6}^{\infty} \begin{Bmatrix} a_{n+1}(c+n)(c+n-1)(c+n-2)(c+n-3)(c+n-4)(c+n-5) \\ +a_{n-1}(c+n-2)(c+n-3)(c+n-4)(c+n-5)c_1 \\ +a_{n-2}(c+n-3)(c+n-4)(c+n-5)[c_2(c+n-6)+c_4] \\ +a_{n-3}(c+n-4)(c+n-5)[c_3(c+n-6)(c+n-7)+c_5(c+n-6)+c_6] \\ +a_{n-4}(c+n-5)[c_7(c+n-6)+c_9] \\ +a_{n-5}[c_8(c+n-6)(c+n-7)+c_{10}(c+n-6)+c_{11}] \end{Bmatrix}\xi^n \\ &=0 \end{aligned} \tag{21}$$

Relationships between the coefficients a_{n+1} are found by equating the coefficients of ξ^n to zero in equation (21). First, considering the coefficient of ξ^0 gives the inidicial equation

$$a_1c(c-1)(c-2)(c-3)(c-4)(c-5)=0 \tag{22}$$

Because the roots of equation (22) differ by integer values, the general solution can be obtained simply by considering the lowest root $c=0$, see [19], so that a_1 is arbitrary. Next, substituting $c=0$ into the coefficients of ξ, ξ^2, ξ^3, ξ^4 and ξ^5 in equation (21) shows, respectively, that a_2, a_3, a_4, a_5 and a_6 are also arbitrary. Finally, considering the coefficient of ξ^n for $n \geq 6$ gives the following recurrence relationship.

$$a_{n+1} = -\frac{\left\{\begin{array}{l} a_{n-1}(n-2)(n-3)(n-4)(n-5)c_1 \\ +a_{n-2}(n-3)(n-4)(n-5)[c_2(n-6)+c_4] \\ +a_{n-3}(n-4)(n-5)[c_3(n-6)(n-7)+c_5(n-6)+c_6] \\ +a_{n-4}(n-5)[c_7(n-6)+c_9] \\ +a_{n-5}[c_8(n-6)(n-7)+c_{10}(n-6)+c_{11}] \end{array}\right\}}{n(n-1)(n-2)(n-3)(n-4)(n-5)} \tag{23}$$

A similar procedure, by substituting equation (19) into equation (16), leads to $\bar{c} = 0$ and thus proceeding in the same way as above, it can be shown that the first six coefficients b_1, b_2, b_3, b_4, b_5 and b_6 of equation (19) are arbitrary, while for $n \geq 6$,

$$b_{n+1} = -\frac{\left\{\begin{array}{l} b_{n-1}(n-2)(n-3)(n-4)(n-5)c_1 \\ +b_{n-2}(n-3)(n-4)(n-5)[c_2(n-6)+\bar{c}_4] \\ +b_{n-3}(n-4)(n-5)[c_3(n-6)(n-7)+\bar{c}_5(n-6)+\bar{c}_6] \\ +b_{n-4}(n-5)[c_7(n-6)+c_9] \\ +b_{n-5}[c_8(n-6)(n-7)+c_{10}(n-6)+c_{11}] \end{array}\right\}}{n(n-1)(n-2)(n-3)(n-4)(n-5)} \tag{24}$$

Supposing that the infinite series of equations (18) and (19) are each truncated to their first N terms, one can write

$$\mathbf{a} = \begin{bmatrix} a_1 \\ a_2 \\ \vdots \\ a_N \end{bmatrix}; \qquad \mathbf{b} = \begin{bmatrix} b_1 \\ b_2 \\ \vdots \\ b_N \end{bmatrix}; \qquad \mathbf{A} = \begin{bmatrix} a_1 \\ a_2 \\ a_3 \\ a_4 \\ a_5 \\ a_6 \end{bmatrix}; \qquad \mathbf{B} = \begin{bmatrix} b_1 \\ b_2 \\ b_3 \\ b_4 \\ b_5 \\ b_6 \end{bmatrix} \tag{25}$$

In this way, all the coefficients of the series in equations (18) and (19) can be expressed in terms of the arbitrary ones, i.e.

$$\mathbf{a} = \mathbf{A}_U\mathbf{A}\,; \qquad \mathbf{b} = \mathbf{A}_V\mathbf{B} \tag{26}$$

where the first six rows of $\mathbf{A}_U$ and $\mathbf{A}_V$ each form a unit matrix, and the remaining rows are obtained from the recurrence relations of equations (23) and (24), respectively.

Now, from equation (10),

$$V = i\alpha_6(U'' + \alpha_1 U) \tag{27}$$

where

$$\alpha_6 = \frac{k_u}{2\omega\Omega L^2} \tag{28}$$

and so, by comparing the coefficients of the first six powers of ξ, one obtains

$$\mathbf{B} = i\alpha_6 \mathbf{T}\mathbf{A} \tag{29}$$

where

$$\mathbf{T} = \begin{bmatrix} \alpha_1 & 0 & 2 & 0 & 0 & 0 \\ 0 & \alpha_1 & 0 & 6 & 0 & 0 \\ 0 & 0 & \alpha_1 & 0 & 12 & 0 \\ 0 & 0 & 0 & \alpha_1 & 0 & 20 \\ -\frac{c_{11}}{24} & -\frac{c_9}{24} & -\frac{c_6}{12} & -\frac{c_4}{4} & (\alpha_1 - c_1) & 0 \\ 0 & -\frac{(c_{10}+c_{11})}{120} & -\frac{(c_7+c_9)}{60} & -\frac{(c_5+c_6)}{20} & -\frac{(c_2+c_4)}{5} & (\alpha_1 - c_1) \end{bmatrix} \tag{30}$$

Referring to the sign conventions of Figure 3 and the boundary conditions of the beam shown in Figure 4, the displacement and force vectors at ends 1 and 2 of the beam can be written as

$$\boldsymbol{\delta} = \begin{bmatrix} U_1 \\ V_1 \\ \theta_1 \\ U_2 \\ V_2 \\ \theta_2 \end{bmatrix}; \qquad \mathbf{F} = \begin{bmatrix} F_1 \\ S_1 \\ M_1 \\ F_2 \\ S_2 \\ M_2 \end{bmatrix} \tag{31}$$

Now the boundary conditions for displacements and forces can be applied at the two ends of the beam where $\xi = 0$ (i.e. $x = 0$) and $\xi = 1$ (i.e. $x = L$), respectively in order to develop the dynamic stiffness matrix.

Boundary conditions for responses are

$$\left.\begin{array}{llll} \text{At } \xi = 0: & U = U_1; & V = V_1; & \theta = V'(0) = \theta_1; \\ \text{At } \xi = 1: & U = U_2; & V = V_2; & \theta = V'(1) = \theta_2 \end{array}\right\} \tag{32}$$

These boundary conditions are now applied to equations (18) and (19) to give

$$\left.\begin{array}{ll} U_1 = a_1; & U_2 = \sum_{n=1}^{N} a_n; \\ V_1 = b_1; & V_2 = \sum_{n=1}^{N} b_n \\ \theta_1 = b_2/L; & \theta_2 = \sum_{n=1}^{N} (n-1) b_n / L \end{array}\right\} \tag{33}$$

The following boundary conditions for loads are obtained by applying equations (7) and noting that $f = Fe^{i\omega t}$, $s = Se^{i\omega t}$ and $m = Me^{i\omega t}$ where F, S and M are the amplitudes of axial force, shear force and bending moment.

$$\left.\begin{aligned} &\text{At } \xi = 0: \quad F = -F_1\,; \quad S = \frac{EI}{L^3}V'''(0) = S_1\,; \quad M = -\frac{EI}{L^2}V''(0) = M_1\,; \\ &\text{At } \xi = 1: \quad F = F_2\,; \quad S = \frac{EI}{L^3}V'''(1) = -S_2\,; \quad M = -\frac{EI}{L^2}V''(1) = -M_2 \end{aligned}\right\} \quad (34)$$

Thus the above boundary conditions for forces give

$$\left.\begin{aligned} &F_1 = \frac{EA}{L}(a_2)\,; \qquad F_2 = -\frac{EA}{L}\sum_{n=1}^{N}(n-1)a_n\,; \\ &S_1 = \frac{EI}{L^3}\left\{6b_4 - \left[\alpha_3\left(r_0 + \frac{1}{2}\right) + \alpha_5\right]b_2\right\}\,; \\ &S_2 = -\frac{EI}{L^3}\sum_{n=1}^{N}(n-1)[(n-2)(n-3) - \alpha_5]b_n\,; \\ &M_1 = -\frac{EI}{L^2}(2b_3)\,; \qquad M_2 = \frac{EI}{L^2}\sum_{n=1}^{N}(n-1)(n-2)b_n \end{aligned}\right\} \quad (35)$$

Equations (33) and (35) can be expressed in matrix form as follows.

$$\boldsymbol{\delta} = \mathbf{Q}_a\mathbf{a} + \mathbf{Q}_b\mathbf{b}\,; \qquad \mathbf{F} = \mathbf{R}_a\mathbf{a} + \mathbf{R}_b\mathbf{b} \quad (36)$$

Substituting equations (26) into equations (36) and using equation (29) gives

$$\boldsymbol{\delta} = \mathbf{QA}\,; \qquad \mathbf{F} = \mathbf{RA} \quad (37)$$

where

$$\mathbf{Q} = \mathbf{Q}_a\mathbf{A}_U + i\alpha_6\mathbf{Q}_b\mathbf{A}_V\mathbf{T}\,; \qquad \mathbf{R} = \mathbf{R}_a\mathbf{A}_U + i\alpha_6\mathbf{R}_b\mathbf{A}_V\mathbf{T} \quad (38)$$

The dynamic stiffness matrix **K** for the rotating beam, which relates the amplitudes of the forces **F** to those of the displacements **δ** can now be obtained by eliminating the constant vector **A** from equation (37) to give

$$\mathbf{F} = \mathbf{K}\boldsymbol{\delta} \quad (39)$$

where

$$\mathbf{K} = \mathbf{R}\mathbf{Q}^{-1} \tag{40}$$

is the required dynamic stiffness matrix. Clearly **K** is a complex Hermitian matrix comprising pure real and pure imaginary elements in the following form. Thus

$$\mathbf{K} = \begin{bmatrix} k_{11} & 0 & 0 & k_{14} & 0 & 0 \\ 0 & k_{22} & k_{23} & 0 & k_{25} & k_{26} \\ 0 & k_{23} & k_{33} & 0 & k_{35} & k_{36} \\ k_{14} & 0 & 0 & k_{44} & 0 & 0 \\ 0 & k_{25} & k_{35} & 0 & k_{55} & k_{56} \\ 0 & k_{26} & k_{36} & 0 & k_{56} & k_{66} \end{bmatrix} + i \begin{bmatrix} 0 & k_{12} & k_{13} & 0 & k_{15} & k_{16} \\ -k_{12} & 0 & 0 & k_{24} & 0 & 0 \\ -k_{13} & 0 & 0 & k_{34} & 0 & 0 \\ 0 & -k_{24} & -k_{34} & 0 & k_{45} & k_{46} \\ -k_{15} & 0 & 0 & -k_{45} & 0 & 0 \\ -k_{16} & 0 & 0 & -k_{46} & 0 & 0 \end{bmatrix} \tag{41}$$

where each term k_{ij} is real. In other words, **K** is a real symmetric stiffness matrix in which the axial and flexural components are uncoupled, augmented by an imaginary Hermitian matrix coupling these behaviours.

3. Application of the Dynamic Stiffness Matrix

The dynamic stiffness matrix **K** of equation (41) can now be used to compute the natural frequencies and mode shapes of either an individual rotating beam or an assembly of them. Once the overall dynamic stiffness matrix of the final structure consisting of rotating beams is assembled, the Wittrick-Williams algorithm [17] is applied in the following manner to determine the natural frequencies of the structure.

(i) For an arbitrarily chosen trial frequency ω^*, the dynamic stiffness matrix $\mathbf{K}_f(\omega^*)$ of the final structure is computed first and then the matrix is triangulated into upper diagonal form $\mathbf{K}_f^{\Delta}$ by using Gauss elimination. Then the number of negative elements on the leading diagonal of $\mathbf{K}_f^{\Delta}$ is counted. This so-called sign count $s\{\mathbf{K}_f\}$ is an integral part of the algorithm which gives an indication of the number of natural frequencies lying below the trial frequency ω^*.

(ii) Since the DSM for free vibration analysis is exact, it allows an infinite number of natural frequencies to be accounted for when all nodes of the structures are fully clamped so that one

or more individual elements in the structure can still vibrate freely on their own between the nodes. This happens when the displacement vector **D** to which $\mathbf{K}_f(\omega^*)$ corresponds is null, and gives rise to the so-called j_0 count of the algorithm, which is essentially the number of clamped-clamped natural frequencies of all individual elements in the structure exceeded by the trial frequency ω^*. The j_0 count is an important part of the algorithm and is not always a peripheral issue. However, for most practical applications, the clamped-clamped natural frequencies of individual elements are generally very high, and thus they are not usually exceeded by any practical trial frequency ω^*, so that j_0 is zero. As a consequence, the analysis is predominantly based on the sign count $s\{\mathbf{K}_f\}$ of (i) above. One of the ways to avoid the computation of j_0 is to split the elements into a number of smaller elements for which the clamped-clamped natural frequencies will be exceptionally high, resulting into zero values for j_0 at all frequencies of interest.

When the integer numbers given by $s\{\mathbf{K}_f\}$ and j_0 of (i) and (ii), respectively, are added together to give j, it can be stated with certainty [17] that j is the total number of natural frequencies of the structure lying below the trial frequency ω^*. It should thus be noted that the Wittrick-Williams algorithm does not give the numerical values of the natural frequencies directly, but it shows how many of them exist below an arbitrarily chosen trial frequency. This simple feature of the algorithm can be exploited to advantage by choosing successive trial frequencies to bracket any natural frequency to any desired accuracy. The algorithm, unlike its proof, is thus very simple to implement in a computer program. For a known natural frequency, the mode shapes are subsequently computed by choosing one displacement component of a node and then determining the rest of the displacements in terms of the chosen one.

4. Numerical Results and Discussion

In order to make the application sufficiently general, numerical results are presented in non-dimensional forms, particularly by defining the following non-dimensional parameters.

$$\eta = \Omega \sqrt{\frac{\rho A L^2}{EA}} = \sqrt{(\alpha_1 - \alpha_4)}\,; \qquad \lambda_i = \omega_i \sqrt{\frac{\rho A L^2}{EA}} = \sqrt{\alpha_4}\,; \qquad \sigma = L \sqrt{\frac{k_u}{k_v}} \tag{42}$$

where η is the non-dimensional rotational speed, λ_i is the non-dimensional natural frequency and σ is the slenderness ratio of the beam, with k_u and k_v defined in equation (9). The non-dimensional hub radius $r_0 = r_h/L$ of equation (15) has also been used as a parameter when obtaining the results using the present theory. Results with and without the inclusion of Coriolis effects have been designated as Case A and Case B, respectively. The Case B results were obtained using the earlier dynamic stiffness theory developed by the first author [1].

The first five non-dimensional natural frequencies λ_i $(i = 1, 2, \ldots, 5)$ of the rotating beam for cantilever boundary condition are shown in Table 1 for a wide range of the non-dimensional speed parameter η, when the slenderness ratio σ is set to 100 and the hub radius parameter r_0 is set to zero. Clearly for Case B when the Coriolis effects are ignored, the flexural and axial motions are uncoupled. Thus the natural frequencies corresponding to the flexural motion will always increase due to the centrifugal stiffening effect from the rotational speed, whereas those corresponding to axial motion will remain unaltered, as expected. This is evident from the results shown in Table 1 where $\lambda = 1.57080$ (i.e. $\pi/2$) corresponds to the fundamental axial natural frequency of the beam with cantilever boundary condition. In the Case B results, the numerical values of these axial natural frequencies are unaffected as a result of the centrifugal action, but their positions in terms of the order of the natural frequencies are altered when the rotational speed increases because of the increase in the bending natural frequencies. Focusing on the results given in Table 1, it is clear that when the Coriolis effects are included (i.e. the Case A results), both the bending and the axial natural frequencies change, particularly at high rotational speeds because the two motions are coupled through Coriolis effects. The results indicate that the influence of the Coriolis effects on the natural frequencies is pronounced only at high rotational speeds (η exceeding 0.5). Comparison of Case A and Case B results in Table 1 shows that the Coriolis effects diminish the natural frequencies, as observed by other researchers [5, 16].

The next set of computations was carried out to validate the DSM theory of this paper and to illustrate its predictable accuracy. This is achieved by comparing results from the present theory with those available in the literature. Table 2 shows the first five non-dimensional natural frequencies of a rotating cantilever beam with the inclusion of Coriolis effects for three different values of slenderness ratio σ alongside the results of Huang et al [16] when $\eta = 0.1$ and $r_0 = 0$. The results are in complete agreement as can be seen.

In order to demonstrate the effect of hub radius, Table 3 shows the first three non-dimensional natural frequencies of the cantilever rotating beam when $\eta = 0.05$ and $\sigma = 1000$ for which some comparative results using Timoshenko beam theory are available in the literature [5]. Clearly for such a high value of the slenderness ratio σ, the results are expected to be close and indeed, they are really very close as can be seen in Table 3.

The next set of results was obtained to illustrate the mode shapes of the rotating beam with the inclusion of the Coriolis effects. Figure 5 shows the first five modes of the beam with cantilever boundary condition when $\eta = 0.05$, $r_0 = 0$ and $\sigma = 100$. It is evident that the first four modes are essentially bending modes whereas the fifth mode is an axial one with a small amount of bending displacement present. The effect of coupling between the bending and axial modes is not so pronounced in this particular case.

It is interesting to note from the Case A results in Table 1 that allowing for the Coriolis effects, and hence coupling the axial and bending behaviour, appears to counterbalance the stiffening effect arising from the rotating action. Thus, for exceptionally high rotational speeds (η), the lowest in-plane natural frequency of the rotating beam begins to decrease with increasing rotational speed. In order to capture this effect and its trend, Figure 6 shows the variation of the lowest natural frequency (λ_1) of the rotating beam against η when $r_0 = 0$ and $\sigma = 100$ for the cantilever boundary condition. For small values of η, λ_1 increases and it peaks at around $\eta = 0.6$ for this particular case. Then λ_1 gradually decreases and becomes zero when η is close to $\pi/2$. This phenomenon does not occur for the Case B results in Table 1, in which the coupling effects of the Coriolis terms are excluded so that λ_1 illustrates purely bending behavior. It is therefore consistent with the apparent axial instability at $\eta = \pi/2$ previously observed by Hodges and Bless [20], which they explained to be a consequence of the use of linear small deflection theory at strain levels well beyond the limits of linear

theories for practical engineering materials. Allowing for non-linear strain terms would reverse this trend and hence avoid the prediction of instability, but it is believed that such a refinement is not necessary for many practical applications of beams rotating at realistic speeds.

The results shown in Table 1 also reveal some interesting modal interchanges or modal flip-over phenomena where bending and axial modes switch (cross) over. The fourth and fifth natural frequencies (λ_4 and λ_5) of the rotating cantilever beam switch over at around $\eta = 0.2$ which is illustrated in Figure 7. Below $\eta = 0.2$, the fourth mode is predominantly bending and the fifth one is axial whereas above this rotational speed at $\eta = 0.3$, the fourth mode is predominantly axial and the fifth one is bending. At $\eta = 0.2$, the modes are somewhat coupled in bending and axial motion, particularly the fourth mode. In order to gain some insight, the fourth and the fifth modes for $\eta = 0.1$, 0.2 and 0.3 are plotted in Figure 8. The modal interchanges as a consequence of the inclusion of the Coriolis effects are clearly evident.

5. Scope and Limitations of the Theory

The dynamic stiffness theory presented in this paper is based on Bernoulli-Euler beam model which does not take into account the effects of shear deformation and rotatory inertia. To account for these effects, the application of the Timoshenko beam theory will be more appropriate. To this end the dynamic stiffness development of a rotating Timoshenko beam with the inclusion of Coriolis effects will be an enormously difficult, but a challenging task, constituting the subject matter of future research. This useful extension will be of great value in predicting accurately the free vibration behaviour of rotating beams with the inclusion of Coriolis effects. Also the present theory considers in-plane flexural free vibration of the rotating beam and the axial deformation is assumed to be coupled only through Coriolis effects with no other forms of coupling effects are present. Obviously the out of plane flexure and torsional deformations are disregarded in the analysis.

Furthermore, as a consequence of using linear small deflection theory when formulating the dynamic stiffness matrix, all nonlinear effects arising from the coupling between various modes of deformation, particularly the axial-bending nonlinear coupling and the stiffening effect due to rotation, have been ignored. In order to explore the effects of nonlinearities of

both geometric and dynamic origin when investigating the free vibration characteristics of rotating beams, interested readers are referred to the works of Turhan and Bulut [21], Lacarbonara *et al* [22], Arvin *et al* [23], Kim *et al* [24] and Sotoudeh and Hodges [25, 26].

6. Conclusions

By using Hamilton's principle, the governing differential equations of motion of a rotating beam for its lag-wise motion which couples the flexural and axial deformations through Coriolis effects have been derived and solved using the Frobenius method of series solution. Then a systematic procedure has been devised to derive the dynamic stiffness matrix of the rotating beam. The ensuing dynamic stiffness matrix has been used through the application of the Wittrick-Williams algorithm to investigate its free vibration characteristics with cantilever boundary condition. Results are given for a wide range of rotational speeds and hub radius ratios. The effect of each of these parameters on the free vibration behaviour has been examined and demonstrated. At high rotational speed, the coupling between bending and axial deformations can be significant. An instability which shows how the natural frequency diminishes due to Coriolis effects has been captured. Some representative mode shapes are also presented. The investigation has shown that for high rotational speeds modal interchanges due to the Coriolis effects occur, affecting the order and magnitude of the natural frequencies. The proposed dynamic stiffness theory is accurate and computationally efficient and can be used to analyse a non-uniform rotating beam by modelling it as a collection of uniform beams with different properties, but with collinear neutral axes. The theory can also be used as an aid to validate finite element and other approximate methods.

References

1. J.R. Banerjee, Free vibration of centrifugally stiffened uniform and tapered beams using the dynamic stiffness method, *Journal of Sound and Vibration*, 233 (5) (2000) 857-875.
2. S.M. Hashemi, M.J. Richard, Natural frequencies of rotating uniform beams with Coriolis effects, *Transactions of the ASME, Journal of Vibration and Acoustics*, 123 (4) (2001) 444-455.
3. K.J. Huang, T.S. Liu, Dynamic analysis of rotating beams with nonuniform cross sections using the dynamic stiffness method, *Transactions of the ASME, Journal of Vibration and Acoustics*, 123 (4) (2001) 536-539.

4. J.R. Banerjee, Dynamic stiffness formulation and free vibration analysis of centrifugally stiffened Timoshenko beams, *Journal of Sound and Vibration***,** 247 (1) (2001) 97-115.
5. S.C. Lin, K.M. Hsiao, Vibration analysis of a rotating Timoshenko beam, *Journal of Sound and Vibration*, 240 (2) (2001) 303-322.
6. J. Chung, H.H. Yoo, Dynamic analysis of a rotating cantilever beam by using the finite element method, *Journal of Sound and Vibration*, 249 (1) (2002) 147-164.
7. H.H. Yoo, S. Seo, K. Huh, The effect of a concentrated mass on the modal characteristics of a rotating cantilever beam, *Proceedings of the Institution of Mechanical Engineers Part C, Journal of Mechanical Engineering Science*, 216 (2) (2002) 151-163.
8. G. Wang, N.M. Wereley, Free vibration analysis of rotating blades with uniform tapers, *AIAA Journal*, 42 (12) (2004) 2429-2437.
9. J.R. Banerjee, H. Su, D.R. Jackson, Free vibration of rotating tapered beams using the dynamic stiffness method, *Journal of Sound and Vibration*, 298 (4-5) (2006) 1034-1054.
10. K.G. Vinod, S. Gopalakrishnan, R. Ganguli, Free vibration and wave propagation analysis of uniform and tapered rotating beams using spectrally formulated finite elements, *International Journal of Solids and Structures*, 44 (18-19) (2007) 5875-5893.
11. S.Y. Lee, J.J. Sheu, Free vibration of an extensible rotating inclined Timoshenko beam, *Journal of Sound and Vibration*, 304 (3-5) (2007) 606-624.
12. O. O. Ozgumus, M.O. Kaya, Energy expressions and free vibration analysis of a rotating double tapered Timoshenko beam featuring bending-torsion coupling, *International Journal of Engineering Science*, 45 (2-8) (2007) 562-586.
13. J. Baba Gunda, R. Ganguli, New rational interpolation functions for finite element analysis of rotating beams, *International Journal of Mechanical Sciences*, 50 (3) (2008) 578-588.
14. O. O. Ozgumus, M.O. Kaya, Flapwise bending vibration analysis of a rotating double-tapered Timoshenko beam, *Archives of Applied Mechanics*, 78 (5) (2008) 379-392.
15. O. O. Ozgumus, M.O. Kaya, Vibration analysis of a rotating tapered Timoshenko beam using DTM, *Meccanica*, 45 (1) (2010) 33-42.
16. C.L. Huang, W.Y. Lin, K.M. Hsiao, Free vibration analysis of rotating Euler beams at high angular velocity, *Computers and Structures*, 88 (17-18) (2010) 991-1001.
17. W.H. Wittrick, F.W. Williams, A general algorithm for computing natural frequencies of elastic structures, *Quarterly Journal of Mechanics and Applied Mathematics***,** 24 (3) (1971) 263-284.

18. W.P. Howson, F.W. Williams, Natural frequencies of frames with axially loaded Timoshenko members, *Journal of Sound and Vibration*, 26 (4) (1973) 503-515.
19. K.A. Stroud, *Advanced Engineering Mathematics*, Palgrave Macmillan, Basingstoke, 4th edition, 2003, pp. 294-297.
20. D.H. Hodges, R.R. Bless, Axial instability of rotating rods revisited, *International Journal of Non-Linear Mechanics*, 29 (6) (1994) 879-887.
21. O. Turhan, G. Bulut, On nonlinear vibrations of a rotating beam, *Journal of Sound and Vibration*, 322 (1-2) (2009) 314-335.
22. W. Lacarbonara, H. Arvin, F. Bakhtiari-Nejad, A geometrically exact approach to the overall dynamics of elastic rotating blades-part I: linear modal properties, *Nonlinear Dynamics*, 70 (1) (2012) 659-675.
23. H. Arvin, W. Lacarbonara, F. Bakhtiari-Nejad, A geometrically exact approach to the overall dynamics of elastic rotating blades-part II: flapping nonlinear normal modes, *Nonlinear Dynamics*, 70 (3) (2012) 2279-2301.
24. H. Kim, H.H. Yoo, J. Chung, Dynamic model for free vibration and response analysis of rotating beams, *Journal of Sound and Vibration*, 332 (22) (2013) 5917-5928.
25. Z. Sotoudeh, D.H. Hodges, Structural dynamics analysis of rotatory blades using fully intrinsic equations, part I: formulation and verification of single-load-path configurations, *Journal of American Helicopter Society***,** 58 (3) (2013) 032003-1– 032003-9.
26. Z. Sotoudeh, D.H. Hodges, Structural dynamics analysis of rotatory blades using fully intrinsic equations, part II: dual-load-path configurations, *Journal of American Helicopter Society***,** 58 (3) (2013) 032004-1– 032004-9.

Table 1. Effect of rotational speed on the in-plane natural frequencies of a rotating cantilever beam for $r_0 = 0$ and $\sigma = 100$. Case A: Coriolis effects included, Case B: Coriolis effects excluded

η	λ_i	Case A	Case B
0.0	λ_1	0.03516	0.03516
	λ_2	0.22035	0.22035
	λ_3	0.61697	0.61697
	λ_4	1.20902	1.20902
	λ_5	1.57080	1.57080
0.02	λ_1	0.03621	0.03622
	λ_2	0.22525	0.22526
	λ_3	0.62240	0.62241
	λ_4	1.21479	1.21480
	λ_5	1.57118	1.57080
0.05	λ_1	0.04066	0.04074
	λ_2	0.24942	0.24950
	λ_3	0.65006	0.65013
	λ_4	1.24459	1.24466
	λ_5	1.57319	1.57080
0.1	λ_1	0.05010	0.05049
	λ_2	0.32084	0.32120
	λ_3	0.73946	0.73976
	λ_4	1.34483	1.34513
	λ_5	1.58039	1.57080
0.5	λ_1	0.08693	0.10447
	λ_2	1.13276	1.16182
	λ_3	1.79799	1.57080
	λ_4	2.02547	2.04618
	λ_5	3.04221	3.05895
1.0	λ_1	0.07632	0.14666
	λ_2	2.01515	1.57080
	λ_3	2.39141	2.27118
	λ_4	3.66494	3.87019
	λ_5	5.16886	5.56470
1.5	λ_1	0.02769	0.17919
	λ_2	2.57842	1.57080
	λ_3	3.12602	3.38605
	λ_4	4.82897	5.71927
	λ_5	6.16571	8.11300

Table 2. Comparison of results with published literature for a rotating cantilever beam including Coriolis effects for different values of slenderness ratio σ when $r_0 = 0$ and $\eta = 0.1$

σ	λ_i	Present theory	Ref. [16]
20	λ_1	0.17972	0.17972
	λ_2	1.12413	1.12413
	λ_3	1.58132	1.58132
	λ_4	3.11043	3.11043
	λ_5	4.71617	4.71617
50	λ_1	0.08086	0.08086
	λ_2	0.49836	0.49836
	λ_3	1.29965	1.29965
	λ_4	1.58046	1.58046
	λ_5	2.48885	2.48885
100	λ_1	0.05010	0.05010
	λ_2	0.32084	0.32084
	λ_3	0.73946	0.73946
	λ_4	1.34483	1.34483
	λ_5	1.58039	1.58039

Table 3. Effect of hub radius on the natural frequencies of rotating cantilever beam when $\eta = 0.05, \sigma = 1000$. Case A: Coriolis effects included, Case B: Coriolis effects excluded

r_0	λ_i	Case A		Case B	
		Present theory	Ref. [5]	Present theory	Ref. [5]
0	λ_1	0.010427	0.010416	0.010447	0.010437
	λ_2	0.116156	0.116148	0.116182	0.116175
	λ_3	0.204599	-	0.204618	-
1	λ_1	0.061469	0.061463	0.061590	0.061584
	λ_2	0.181795	0.181780	0.181839	0.181824
	λ_3	0.303544	-	0.303574	-
2	λ_1	0.086094	-	0.086264	-
	λ_2	0.228787	-	0.228843	-
	λ_3	0.375370	-	0.375407	-

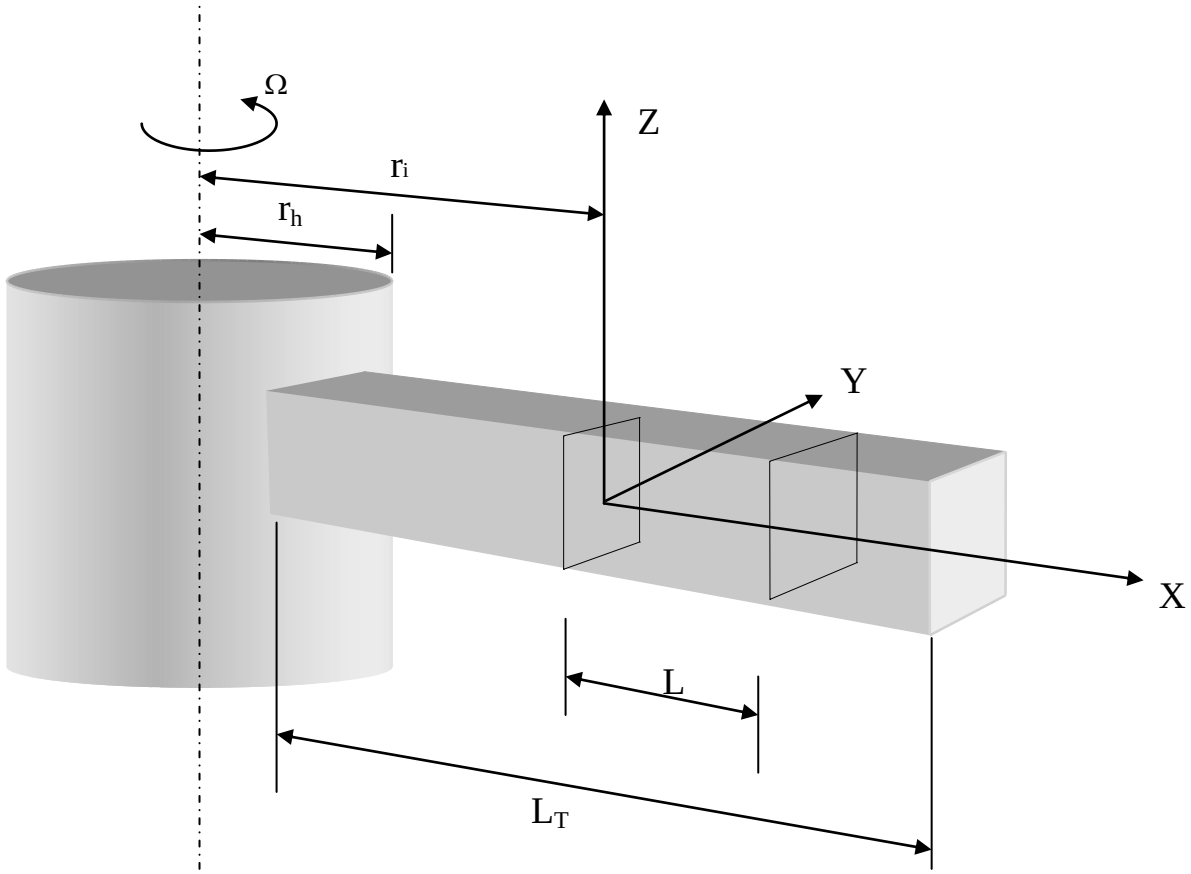

Figure 1. Coordinate system and notation for a rotating Bernoulli–Euler beam

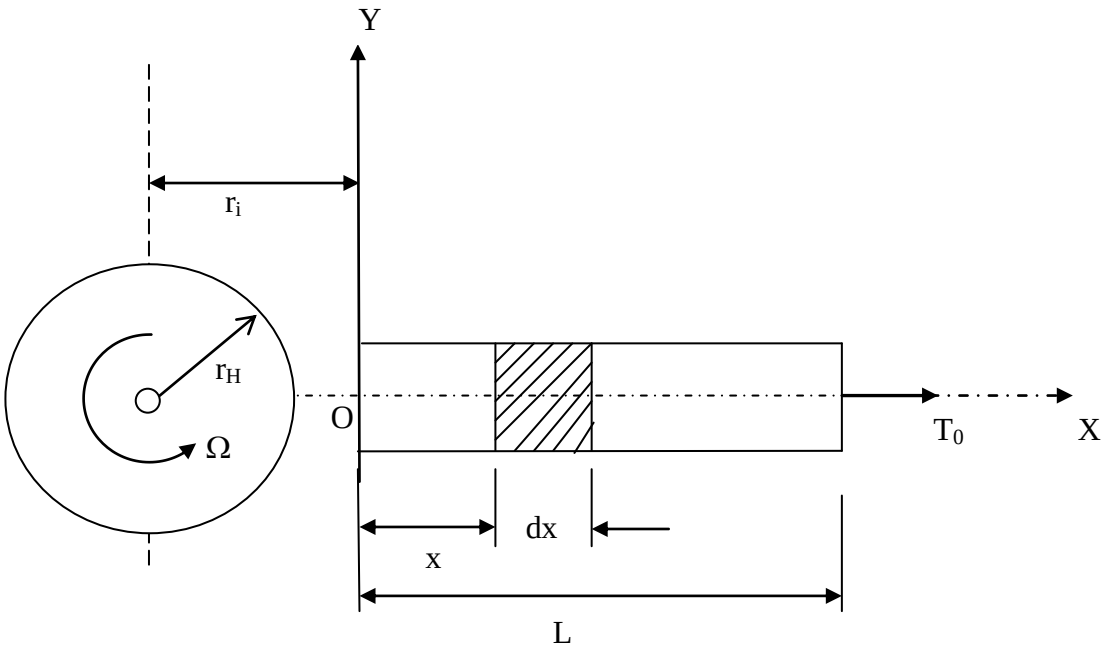

Figure 2. In-plane free vibration of a rotating beam element of length L.

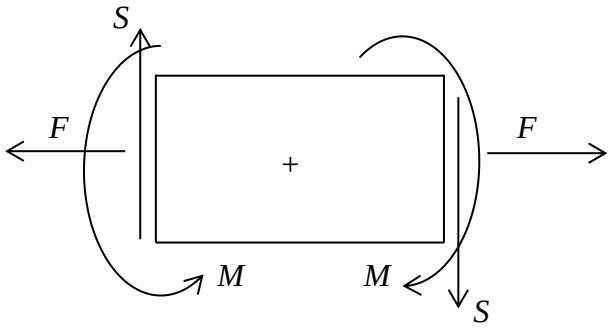

Figure 3. Sign convention for positive axial force (*F*), shear force (*S*) and bending moment (*M*)

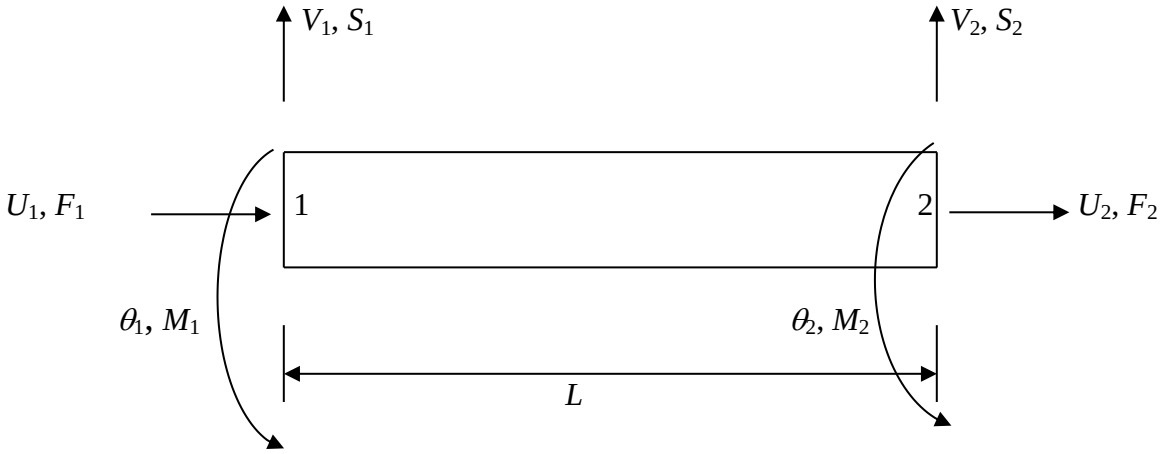

Figure 4. Boundary conditions for displacements and forces of the beam element

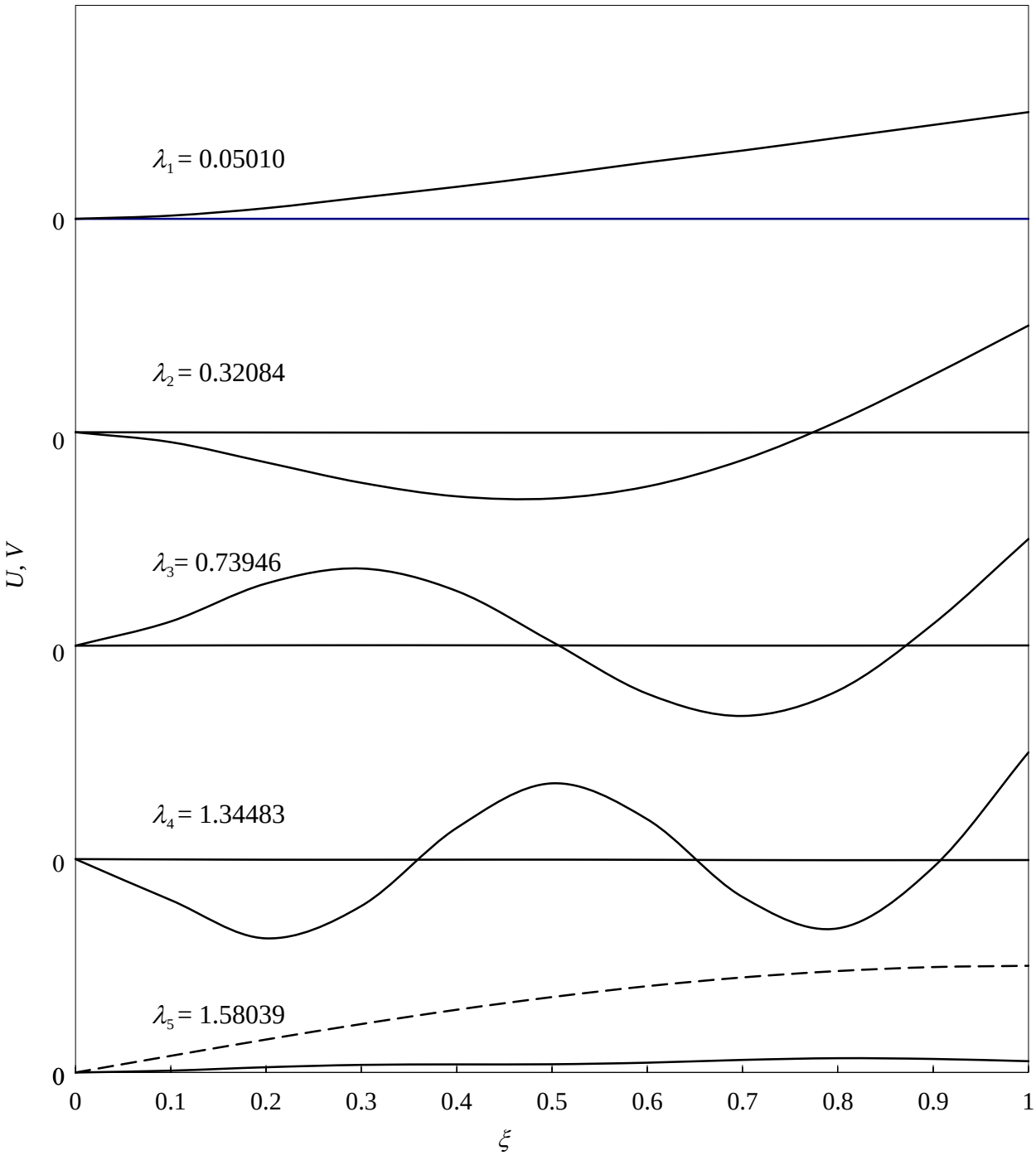

Figure 5. Mode shapes of rotating beam with cantilever boundary condition including Coriolis effects for $\eta = 0.1, r_0 = 0$ and $\sigma = 100$. --------- U ; ——— V

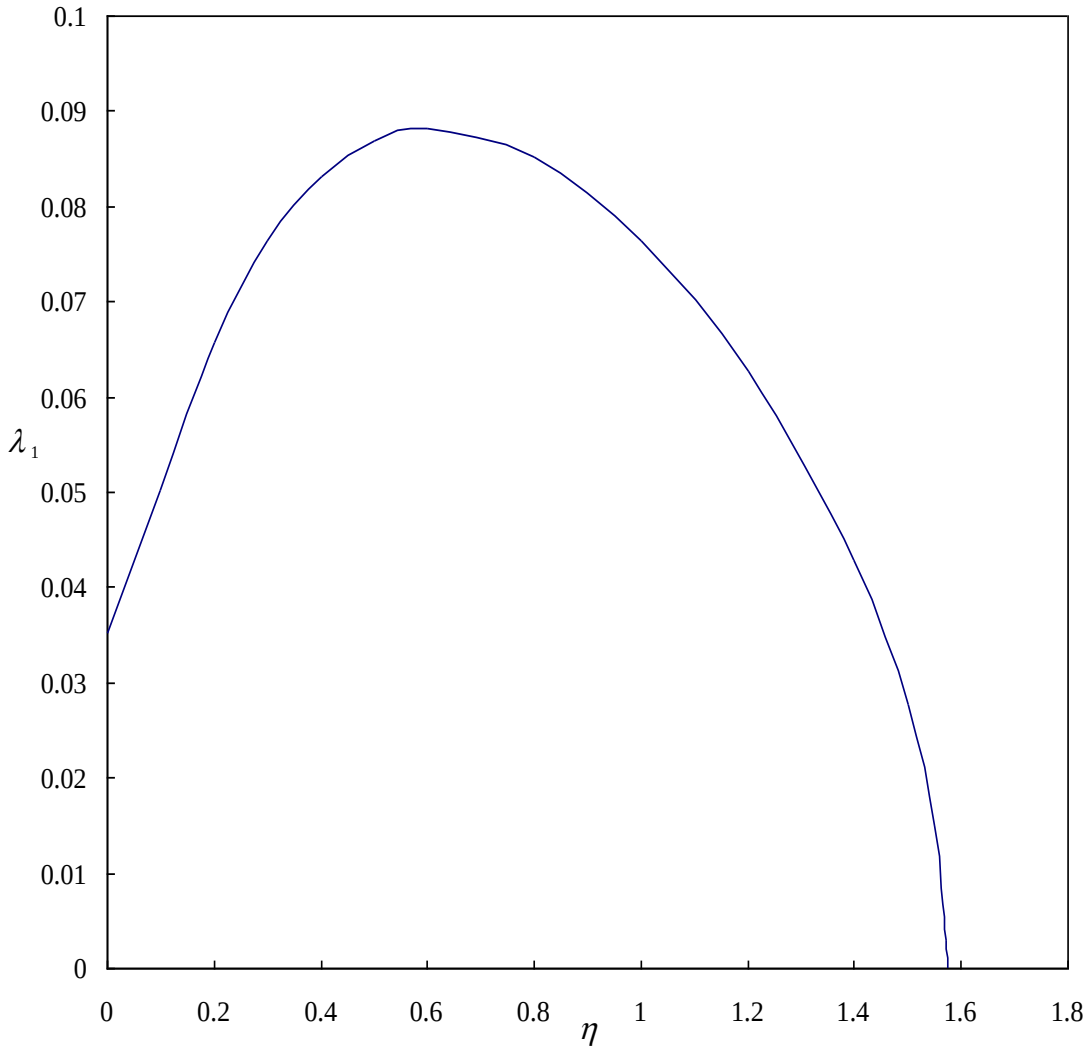

Figure 6. The effect of rotational speed on the fundamental natural frequency of a cantilever rotating beam with the inclusion of Coriolis effects for $r_0 = 0$ and $\sigma = 100$

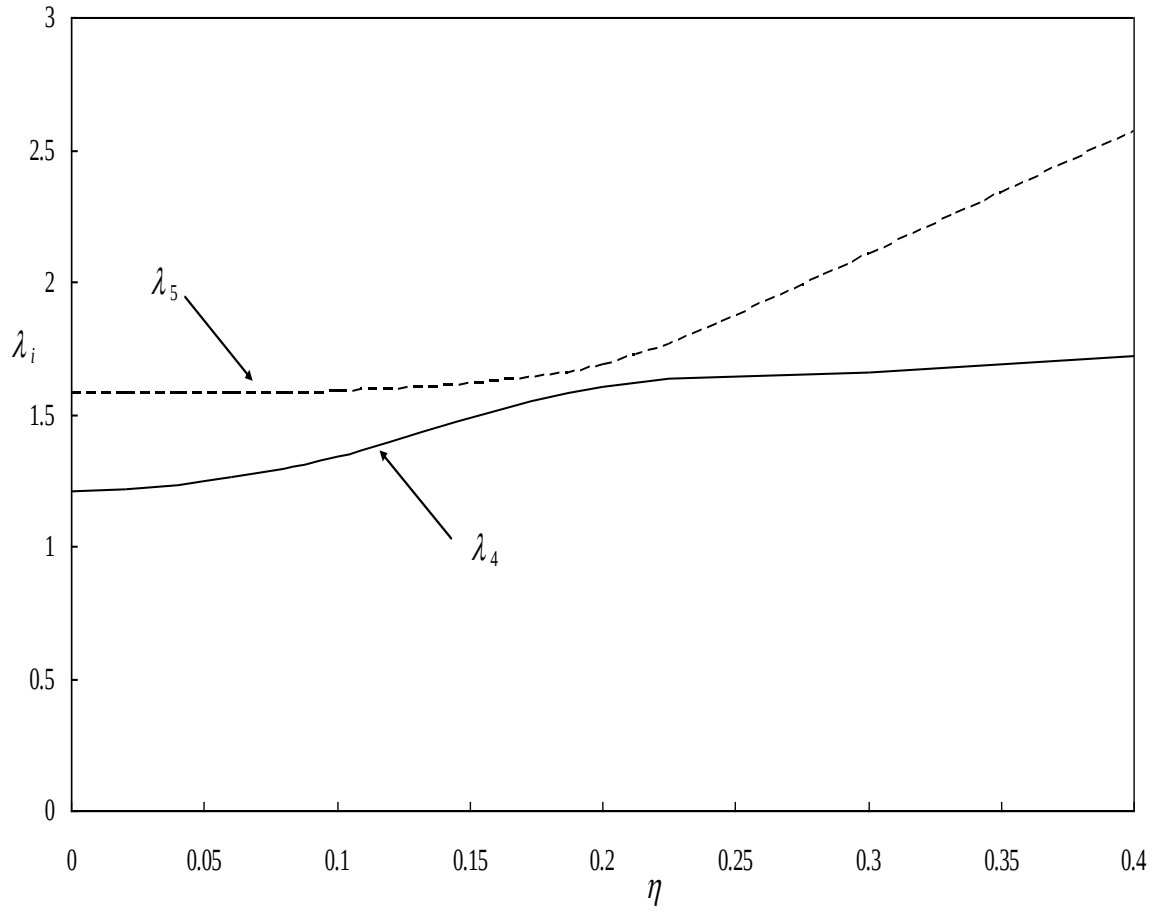

Figure 7. Variation of the fourth and fifth natural frequencies of rotating cantilever beam with rotational speed including Coriolis effects for the case when $r_0 = 0$ and $\sigma = 100$

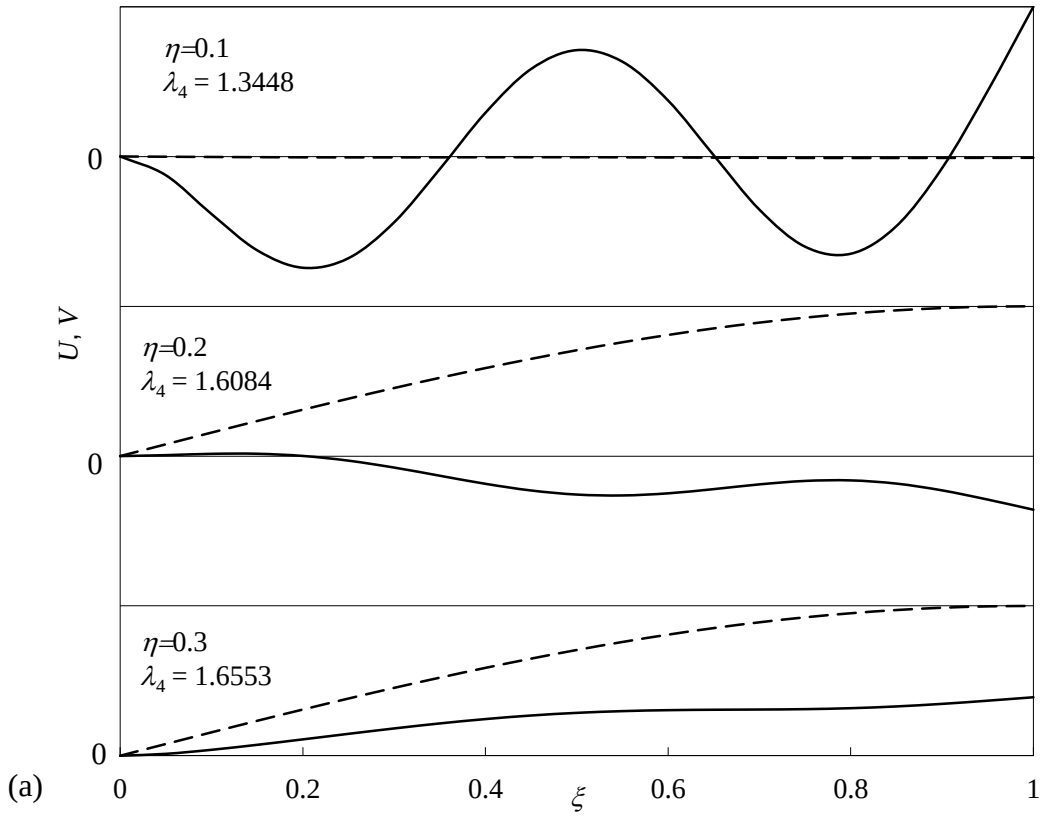

(a)

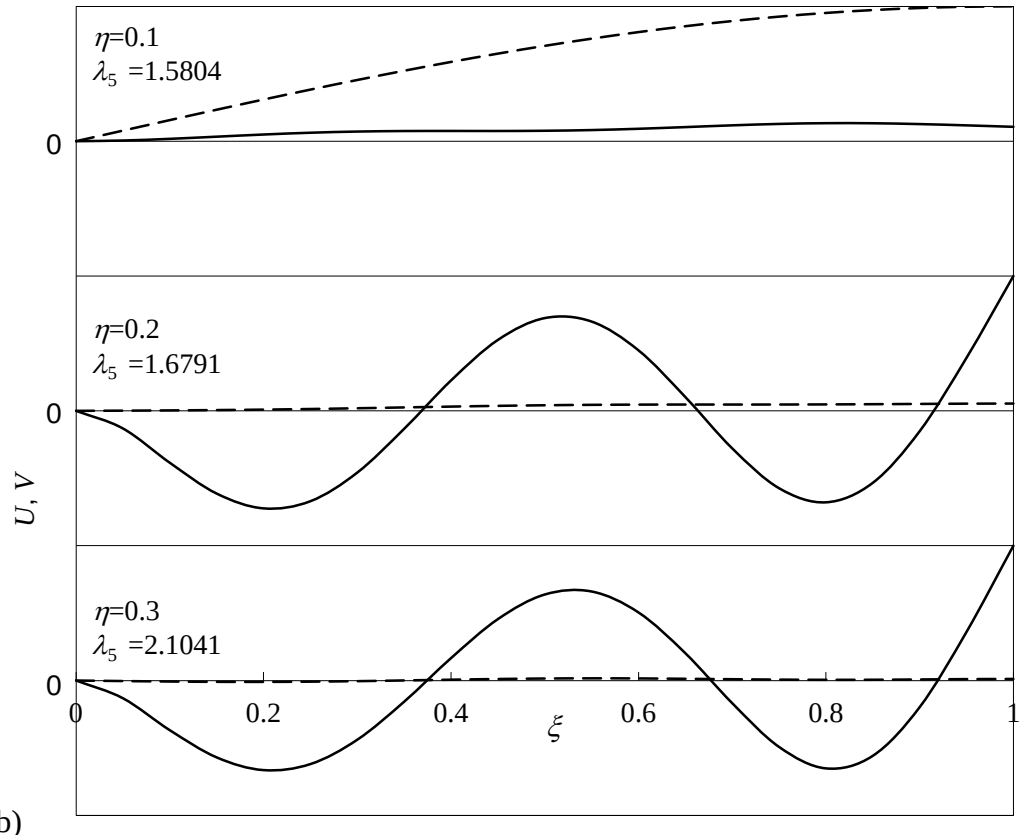

(b)

Figure 8. (a) Fourth and (b) fifth modes of the cantilever beam for different rotational speeds.
---------- U; ———— V